Journal of Non-Crystalline Solids 376 (2013) 43–49

Contents lists available at SciVerse ScienceDirect

Journal of Non-Crystalline Solids

journal homepage: www.elsevier.com/ locate/ jnoncrysol

Spectral UV losses in 355 nm pulsed laser delivery system at low temperatures

J.C. Heimann [a,c], C.P. Gonschior [a,c], K.-F. Klein [a,c,*], G. Hillrichs [b], E. Takala [d]

[a] Technische Hochschule Mittelhessen, Competence Center "Optical Technologies and Systems", Wilhelm-Leuschner-Str. 13, 61169 Friedberg, Germany
[b] Hochschule Merseburg, Geusaer Str. 88, 06217 Merseburg, Germany
[c] TransMIT GmbH, CeFiL, Saarstr. 23, 61169 Friedberg, Germany
[d] CERN, Department TE-MSC, 1211 Geneva 23, Switzerland

ARTICLE INFO

Article history:
Received 20 November 2012
Received in revised form 5 April 2013
Available online xxxx

Keywords:
355 nm pulsed laser;
Multimode fibers;
UV defects;
Precursor;
Low temperatures

ABSTRACT

For a delivery system using high OH polyimide coated all-silica multimode fibers the photo degradation and recovery were investigated for 355 nm pulsed laser radiation at a cryogenic temperature of 77 K (liquid nitrogen) and at room temperature, as reference. For comparison, UV-induced fiber losses generated during light transportation of a deuterium lamp were measured. For these quite different light sources the efficiency of defect generation including UV-induced optical absorption at 214 nm and at 265 nm is significantly different at both temperatures used in these studies. At 77 K, the UV-induced optical loss at 214 nm is significantly reduced, while the same loss at 265 nm is increased, for the tested high OH fibers. In addition, the values of both losses are rapidly changed when the fiber is warmed up from 77 K to room temperature. The observed temperature dependent growth kinetics of UV-induced absorption at 214 nm is considered to be explained by at least two different mechanisms of defect generation.

1. Introduction

Many applications of UV laser radiation at 355 nm wavelength are based on fiber optics. In the past, several details about multimode fiber properties at this wavelength have been investigated [1–3]. The commonly used UV fibers consist of an undoped synthetic silica core and a Fluorine-doped silica cladding, surrounded by a polymer coating. The basic attenuation of these fibers at 355 nm is typical in the order of 0.2 dB/m, while the nonlinear attenuation due to two photon absorption was estimated to be less than 10^{-6} cm/MW [2,4].

Caused by UV irradiation using pulsed 355 nm lasers, additional spectral loss is generated in these fibers in the wavelength region below 300 nm. These UV-induced absorption bands are correlated with two optically active paramagnetic defects in these fibers: the E′ center with an unpaired sp^3 electron on a threefold coordinated Si atom (≡Si•) with an absorption band at 5.8–5.9 eV and the non-bridging oxygen hole center (NBOHC) (≡Si–O•) with an absorption band at 4.8 eV [5–7]. These defect centers are generated from different pre-existing centers (precursors) during the light transportation itself by one- or two-photon absorption. Due to further improvements in manufacturing of preforms and fibers, the concentration of UV defects or precursors after fiber drawing could be significantly reduced in the fiber core, based on high OH (>600 ppm) and low OH (<1 ppm) synthetic silica [8–11]. For these studies and for quality control of improved commercially available material, a setup with broadband deuterium lamp was used to generate UV damage at 214 nm wavelength due to a one-photon process [12,13].

In silica bulk, different kinds of optically active oxygen-deficiency-related E′ centers are supposed to be generated by transformation of precursors, such as non-relaxed oxygen vacancies ODC(II), impurity bonds like Si–H and Si–Cl groups or "strained" Si–O–Si bonds [14–16]. The annealing of defect centers by passivation with molecular hydrogen is a well-known feature of high OH fiber material that is described in details elsewhere [13,17–19]. In high OH silica, a new model for the generation of the optical absorption bands in the wavelength region from 200 nm to 300 nm in high OH silica was proposed [20], taking temperature as a parameter into account.

The passivation of E′ centers in low OH bulk material has been shown to be a thermally activated process [21]. In high OH fibers, hydrogen molecules are available in small concentrations; therefore, the temperature dependent diffusion of hydrogen described in Ref. [22,23] affects the passivation of the UV defects.

The damage of UV fibers with undoped synthetic silica core has been studied in excimer laser delivery systems at room temperature [24,25]. In addition to these lasers at 193, 248 and 308 nm, highly-efficient pulsed or continuous wave lasers based on the 3rd harmonic of Nd:YAG laser at 355 nm wavelength are of commercial interest, too. Because the photon energy is 3.5 eV, the deep-UV defects with absorption at 214 nm (5.8 eV) or 265 nm (4.7 eV) cannot be generated by one-photon absorption in these UV fibers. Although two-photon absorption [2,4] at 355 nm is at least one and a half orders of magnitude

* Corresponding author. Tel.: +49 6031 604 214; fax: +49 6031 604 2082.
E-mail address: Karl-Friedrich.Klein@iem.thm.de (K.-F. Klein).

0022-3093/$ – see front matter © 2013 Elsevier B.V. All rights reserved.
http://dx.doi.org/10.1016/j.jnoncrysol.2013.04.042

lower in comparison to the excimer lasers, the deep-UV defects can be generated. In addition to two-photon processes, two-step processes to generate the optical defects have also been observed in these UV fibers [26], using 355 nm high power pulsed Nd:YAG laser. Based on application requirements, the studies including surface damage [1,27] have commonly been carried out at room temperature.

Due to increasing interest in delivery systems at lower temperatures (liquid nitrogen, liquid helium), such as studying the stability of superconducting strands around 4 K, first results of spectral transmission losses after 355 nm pulsed laser irradiation at cryogenic temperatures have been presented [28,29]. In addition to the generation of defects in fibers (with or without hydrogen loading) at 4 K due to 355 nm irradiation, the bending losses of a 1.2 m long fiber including 4 loops with 25 mm diameter during the cooling-down phase were interesting for the application. At 4 K, a nearly wavelength independent loss of approximately 1.6 dB was measured caused by micro-bending due to the mismatch of thermal expansion of polyimide coating and silica fiber [28].

So far, studies on the photo-darkening and recovery in silica bulk samples, e.g. generation and stability of E′ centers induced by 4.7 eV laser radiation, have been carried out [26,30,31]. In addition, the temperature dependencies and post UV irradiation annealing of E′ centers [19,21] in SiO_2 in the presence of hydrogen, were studied in detail.

In the past, temperature dependent generation and recovery of defects in optical fibers induced by pulsed 355 nm Nd:YAG lasers have not been studied in detail. Stimulated by the application, tests for a light delivery system at 355 nm wavelength were carried out at 4 K (liquid helium) [28,29]. Complimentary to these tests, the following studies will focus on the properties of UV fibers with undoped high OH silica core at 77 K (liquid nitrogen). First results of fiber damage using a 355 nm high pulsed Nd:YAG laser will be shown; in addition to the fiber losses at 355 nm, the spectral UV damage is added. Furthermore, a focus will be on the recovery of UV-induced absorption bands at 77 K and room temperature; especially, the changes of these bands (generated at 77 K) during the short warming-up phase are included. For comparison, the spectral damage of UV fibers irradiated with a deuterium lamp at both temperatures will also be shown.

2. Experimental setup and test fibers

A sketch of the two main setups with principle components is shown in Fig. 1. The first setup consists of a Nd:YAG high pulse power laser system (HPP) as the light source LS. The Flare laser manufactured by InnoLight [32] has the following parameters: 355 nm wavelength, 90 μJ maximum pulse energy, 10 ns pulse width and a maximum repetition rate of 200 Hz. Using an imaging system IS, the laser beam was coupled into the fiber under test FUT. A Dewar flask with liquid nitrogen sustained the FUT with a well-defined bent and two straight sections of approximately 0.2 m at a cryogenic temperature of 77 K. To reduce the influence of the fiber bending, only fibers with 100 μm core and 110 μm cladding diameter were used. Further, two feeding sections with lengths $L_{RT,1}$ of typically 0.3 m were kept necessarily at room temperature; testing a FUT with high UV-induced losses, a low loss feeding fiber was spliced to the FUT. The distal end of the FUT was mounted in front of a detector system DS; in addition to a thermopile power meter (PS19Q, Coherent, Inc. [33]) for measuring average power, pulse energies were evaluated using a pyroelectric detector (PEM100, LTB Berlin GmbH [34]). The fiber end faces were not polished, but cleaved and glued subsequently into SMA connectors C. These connectors were mounted into SMA adapters, placed on translation stages.

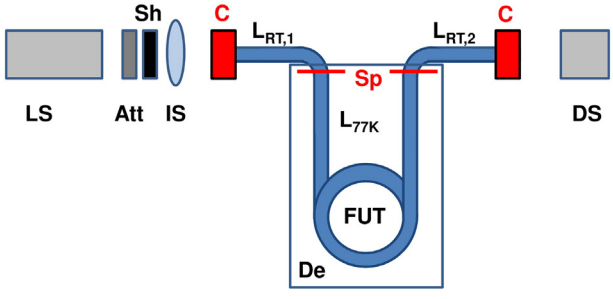

Fig. 1. Measurement setup with principle components; LS: light source (355 nm HPP laser or deuterium-lamp); Att: attenuator; Sh: shutter; IS: imaging system; C: coupling unit including SMA adapter and translation stage; De: Dewar flask; FUT: fiber under test with SMA connector and total length $L_{tot} = L_{RT,1} + L_{RT,2} + L_{77K}$; DS: detector system (thermopile or pyro-electric detector for 355 nm laser; fiber-optic coupled spectrometer); Sp: splice between FUT and feeding fibers of same diameter and cladding core ratio, if needed; only the fiber section with the length L_{77K} is cooled down to 77 K (liquid nitrogen).

In order to avoid mechanical damage of the fiber front face during HPP irradiation, a rotatable dielectric mirror for 355 nm was used as an attenuator Att to adjust the pulse energies. Transmission and reflection of this mirror depend on the rotating angle [1]. For the HPP, the maximum pulse energy coupled into the fiber front face was approximately 20 μJ according to a peak power of 2 kW which leads to a maximum peak power density of 25.5 MW/cm^2, averaged over the fiber core cross-section area. For 4 h tests, the total dose was 367 GJ/cm^2. In addition, a shutter Sh is placed between the light source and the fiber.

All spectral measurements were performed using a standard deuterium (D_2) lamp DO660/05J from Heraeus Noblelight [35] as a broadband light source and an optimized imaging system. The distal end of the FUT is coupled into a fiber-optic spectrometer (FOS) USB4000 from Ocean Optics [36] with UV-enhanced grating for deep-UV used as detector system DS. In order to reduce the noise in the FOS-signal and in the UV-induced loss spectra, either adjacent average with 9 points or Fast-Fourier-Transformation filter smoothing with a cut-off frequency of 0.36 (arb. units) using 15 supporting points was performed after the measurements. This whole system for measuring the spectral UV-induced losses at room temperature is described in details elsewhere [12,13,38].

In the case of fiber damage, the shutter is open and the spectral UV-induced losses L(λ,t) can be easily determined by the wavelength and time-dependent FOS signals [12,13]:

$$L(\lambda, t) = 10 \cdot \log(FOSS(\lambda, t = 0)/FOSS(\lambda, t)) \quad (1)$$

with [L] = dB.

Either the UV-induced loss spectra L(λ) at selected points t_i of time or the time-dependent losses L(t) at selected wavelengths λ_i (e.g. 214, 229, 245, 254, 265, 330 nm) will be derived from the data collected. Because there is no optical absorption band in high OH silica at 330 nm, this wavelength is used to control the stability of the D_2 lamp, especially for long test runs.

The position of the shutter Sh is controlled by software via electrical TTL output of a computer. Two cases will be distinguished. With an open shutter, the photo-darkening of the FUT with D_2 lamp is measured. During recovery after UV damage, the deuterium irradiation is blocked to mainly avoid additional damage. For each measurement point, however, the shutter is opened for 2 … 5 s, only; within this small interval in comparison to the long period of darkness, the UV damage is negligible [12,13,38]. For the following studies at 77 K, the Dewar flask (see Fig. 1) with liquid nitrogen was added to the standard setup. The D_2 lamp DO660/05J from Heraeus Noblelight [35] was mainly used in operation; for comparison, a Hamamatsu D_2 lamp L10290 [38] was used, too, because the spectral power coupled into the fiber was significantly higher for wavelengths >220 nm, as shown in the inset of Fig. 2. In addition to the spectral power, many other wavelength dependent test parameters have to be controlled carefully to receive comparable results in respect to the final saturation level of UV damage, e.g. total running time and electrical current of the lamp, imaging system, position of fiber front face related to a well-defined focal point of a lens system, temperature, duration of test, and fiber length. In the presence of oxygen,

the generated ozone between lamp and fiber input will reduce the deep-UV power significantly in the wavelength region below 195 nm. Due to the degradation of the D_2 lamp itself, there can be slightly lower levels of saturation with longer time of operation; however, this reduction can be compensated for by a higher current generating the UV-emitting plasma in the 0.5 mm aperture.

Two different UV fiber types manufactured by Polymicro Technologies [10] have been examined: standard FVP fiber (1st generation) and FDP fiber (4th generation). These fibers were all-silica multimode fibers (MMF) with undoped high OH (>600 ppm) silica core and F-doped silica cladding leading to a step-index profile. For mechanical strength, the silica fiber is surrounded by a polyimide coating. The core diameter and the numerical aperture of both fibers were 100 μm and 0.22, respectively. The significant improvements within the last years led to the 4th generation of UV fibers with different core diameters. Currently, the commercially available FDP fiber can be specified as follows: the UV-induced defects at 214 nm and 265 nm wavelengths lead to loss levels < 1 dB in 2 m long fiber samples with 200 μm core diameter [9,10]. On the other hand it is known, that these losses increase with decreasing core diameter [10]. For higher resolution, the length of the FDP–FUT was fixed at 5.0 m for the following tests. In meantime, the induced losses in a 100 μm core FDP-fiber could be further reduced by a factor of more than two. For comparison, the FVP-fiber was also examined. Because the UV-induced losses at 214 nm and room temperature are nearly two orders of magnitude higher, the length of the FVP–FUT was fixed at 0.5 m; as pointed out above, two 0.3 m feeding predamaged FDP fibers were spliced on both sides to avoid the significant decrease of spectral power below 225 nm in the FVP–FUT at room temperature.

3. Results

The commonly used D_2 lamp DO660/05J produced by Heraeus Noblelight [35] proved to be very efficient in generation of UV defects in high OH UV fibers below 300 nm. In Fig. 2, only the main absorption band at 214 nm was monitored with a maximum of about 4 dB after 2 h of irradiation, using our standard FUT, and FDP, with 5 m length. After approx. 2 h, the loss at 214 nm is saturated. The 330 nm signal, used for control purposes to see power fluctuations, showed that the stability of the D_2 lamp at this wavelength with less than 0.15 dB is good.

The FOS signals in the inset of Fig. 2 are proportional to the spectral power densities, at one wavelength. However, the transfer factor in the spectrometer, from spectral (input) power to spectral (output) photo-charge, is strongly wavelength dependent. Therefore, the following comparisons are only qualitative. It is obvious, that the spectral power of the Hamamatsu D_2 lamp L10290 [38] was significantly lower in comparison to the Heraeus lamp for wavelengths <210 nm (inset of Fig. 2). As a consequence, the UV-induced loss at 214 nm is significantly lower during the 4 h UV irradiation: the saturation level is not reached, and the gradient of the loss each time is smaller by at least a factor of three.

For determining the length dependent UV-induced attenuation (unit: dB/m) the fiber samples were gradually cut back by 0.5 m several times. Because of low attenuation and the absence of strong UV absorption bands at 355 nm, the power or power density decreases only a small amount over the fiber length (0.5 dB between the input and the output sides). As a consequence, the UV-induced attenuation at 214 nm, generated with the 355 nm HPP laser system, decreases only slightly along the fiber (Fig. 3, left). Using a linear approximation, the regression analysis based on least-squares method leads to the following equation: $\alpha_{UV}(z) = 4.15\ \mathrm{dB/m} - 0.20\ \mathrm{dB/m^2} \cdot z$, with the correlation coefficient $r^2 = 0.326$.

For comparison (Fig. 3, right), the induced attenuation at 214 nm generated with the Heraeus D_2 lamp shows an exponential decrease over the fiber length, from approx. 1.5 dB/m to 0.5 dB/m. The damaging spectrum of the D_2 lamp is significantly changed along the fiber. Especially below 225 nm, the increasing basic attenuation with decreasing wavelength and higher induced attenuation at 214 nm have to be taken into account. Therefore, the exponential decay approximation leads to the following equation: $\alpha_{UV}(z) = 0.85\ \mathrm{dB/m} \cdot \exp(z/0.96\ \mathrm{m}) + 0.56\ \mathrm{dB/m}$ with the correlation coefficient $r^2 = 0.874$.

In Fig. 4, the temperature dependent mechanisms of defect generation in FDP- and FVP–FUT are shown, each after irradiation for 4 h with the Heraeus D_2 lamp. The main absorption band at 214 nm is obvious, with an induced loss of about 3.5 dB (FDP 5.0 m length) and 8.0 dB (FVP 0.5 m length); as shown in Ref. [37], the 214 nm optical absorption is >50 dB for a 4.0 m long FVP-sample. On the other hand, the irradiation in liquid nitrogen at 77 K results in a significantly smaller optical absorption band at 214 nm of 0.3 dB (FVP 0.5 m length) and 2 dB (FDP 5 m length). In addition, at 77 K, the FDP–FUT features an optical absorption band at 265 nm, which did not occur at room temperature at this significant level. Taking the different fiber lengths into account, the FDP fiber [9,10], which has been optimized and improved at room temperature, is not superior at liquid nitrogen temperature (77 K) in comparison to the FVP fiber.

Using the 5 m long FDP-fiber, only, more details about spectral photo-darkening and post-irradiation recovery at different temperatures

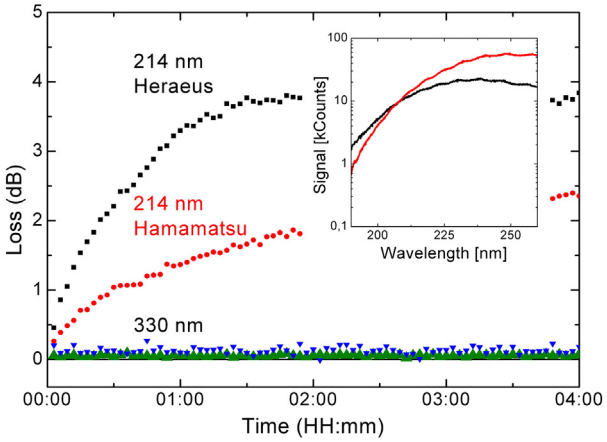

Fig. 2. Growth kinetics of induced losses in 5 m FDP fiber at 214 nm and 330 nm, using different D_2 lamps from different suppliers (Heraeus Noblelight DO660/05J [35], Hamamatsu L10290 [38]); the variation of FOS signal at 330 nm wavelength is monitored to show the drift in the system due to lamp plasma; inset: FOS signal using the two different D_2 lamps, at the beginning of the UV irradiation on a logarithmic scale (details in text).

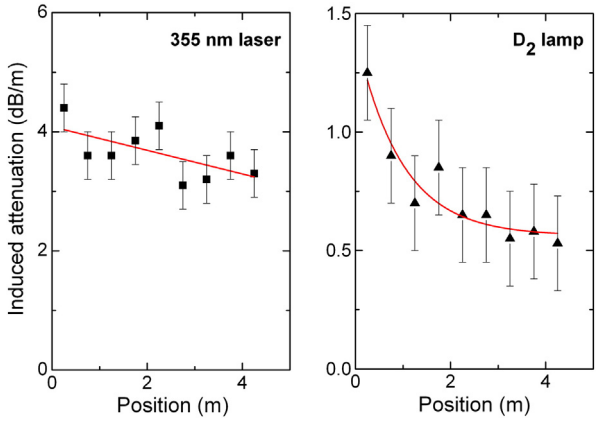

Fig. 3. UV-induced attenuation $\alpha_{UV}(\lambda = 214\ \mathrm{nm}, z)$ at 214 nm in 5 m FDP fiber samples, depending on the fiber position z after 4 h UV irradiation with the 355 nm HPP laser [32] (left diagram) and Heraeus D_2 lamp [35] (right diagram); the selected fitting functions due to regression analyses are: $\alpha_{UV}(z) = 4.15\ \mathrm{dB/m} - 0.20\ \mathrm{dB/m^2} \cdot z$ (linear, left diagram) and $\alpha_{UV}(z) = 0.85\ \mathrm{dB/m} \cdot \exp(z/0.96\ \mathrm{m}) + 0.56\ \mathrm{dB/m}$ (exponential decay, right diagram) with the correlation coefficients $r^2 = 0.326$ and 0.874, respectively.

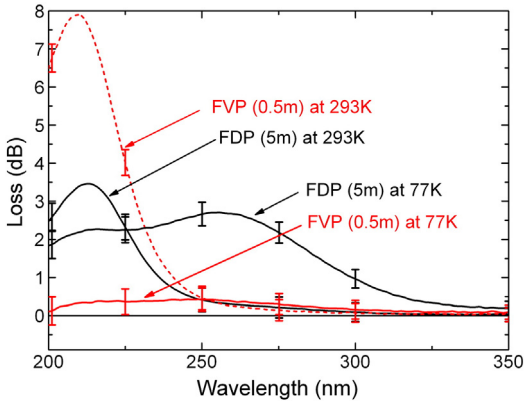

Fig. 4. Comparison of UV-induced losses by irradiation of the 5 m long FDP fiber (solid lines) and the 0.5 m long FVP fiber (dashed lines) using the Heraeus D_2 lamp at room temperature (293 K) and liquid nitrogen temperature (77 K) for 4 h UV-irradiation; the measurement errors are shown for selected wavelengths, calculated with error propagation and estimated variations of FOS signal.

are shown in Fig. 5. First of all, there will be a transmission increase below 210 nm after the cooling-down phase, from room temperature to 77 K (liquid nitrogen). At 200 nm, a gain of 0.20 dB for the 5 m long fiber was measured. After 12 h UV irradiation at 77 K, the optical absorption band at 265 nm is dominant with a value of 5.0 dB; the induced loss of 3.9 dB at 214 nm is smaller compared to the 265 nm loss at 77 K and comparable to the 214 nm loss of 3.5 dB at room temperature in Fig. 4. The same behavior at 77 K is shown in Fig. 4, after 4 h UV irradiation.

Taking the fiber out of the Dewar flask, the fiber was quickly warmed up. After 30 s, the 214 nm loss is higher, while the 265 nm loss is smaller by a factor of two. An additional 4 h recovery at room temperature shows that both absorption bands are reduced; especially the 265 nm loss is below 0.3 dB.

Using a different point of view, the temporal behavior of both absorption bands is shown in Fig. 6. First of all, the losses after 12 h UV irradiation at 77 K are not saturated; still, the values of both slopes are 0.19 dB/h for 214 nm and 0.26 dB/h for 265 nm. Consecutively, the recovery at 77 K and room temperature without continuous UV light was observed. By keeping the fiber in the Dewar flask at 77 K for 12 h, the optical absorption bands decay slightly: the loss reduction at 214 and 265 nm is less than 0.5 dB. However, as soon as the FDP fiber is warmed up to room temperature, a rapid drop followed by an exponential decay of the UV-induced loss at 265 nm is seen. At 214 nm, in contrast, a rapid increase followed by a nearly linear decay is observed. To monitor these abrupt changes more precisely

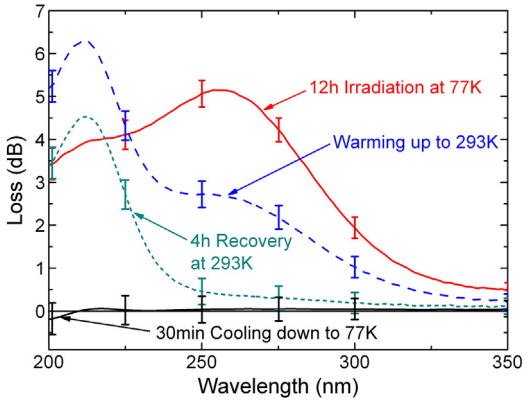

Fig. 5. Spectral UV losses in FDP fiber (5 m length) by UV irradiation with the Heraeus D_2 lamp for 12 h at 77 K (solid line), post-irradiation warming up to 293 K (dashed line) and recovery at room temperature (bold and dashed line); before irradiation, the fiber was cooled down to 77 K showing a transmission gain of the fiber below 210 nm (lowest line).

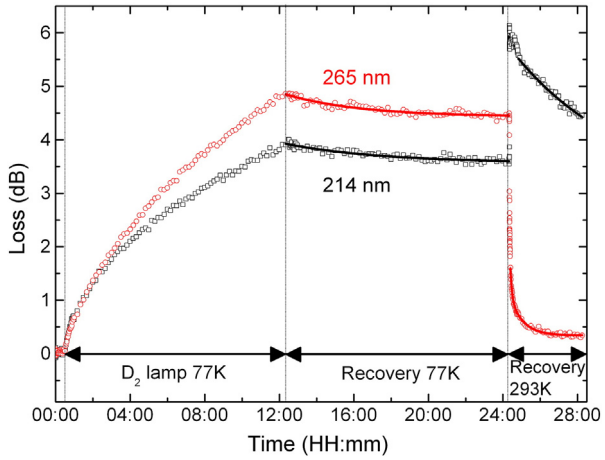

Fig. 6. Kinetics of defect generation at 214 nm and 265 nm for 12 h irradiation of FDP fiber (5 m length) with the Heraeus D_2 lamp at 77 K followed by 12 h annealing at 77 K and 4 h annealing at room temperature (293 K). The vertical dotted lines show the different sections of processing; the recovery at 77 K can be approximated using one exponential decay function as follows: $L(t) = 0.32\ dB \cdot \exp(-t/5.3\ h) + 3.57\ dB$ at 214 nm (lower curve) and $L(t) = 0.45\ dB \cdot \exp(-t/4.0\ h) + 4.43\ dB$ at 265 nm, with the correlation coefficients $r^2 = 0.844$ and 0.887, respectively; the recovery at room temperature, after 24 h total processing time is shown in Fig. 7 in more detail.

during the warming-up phase, the shutter was opened continuously starting 45 s before and 90 s after this step of removing the fiber from the flask.

The warming-up phase from 77 K to room temperature plus the consecutive recovery at room-temperature was studied in more detail (Fig. 7), for different 24 h UV-damaging processes. In case A (see Fig. 6), a 12 h recovery took place after 12 h UV irradiation, in contrast to a 24 h continuous UV irradiation in case B. Because the power level was different in both cases and no saturation was found after 24 h irradiation, the starting values are quite different: 4.3 dB or 14.8 dB at 265 nm and 3.7 or 11.5 dB at 214 nm in cases A and B, respectively.

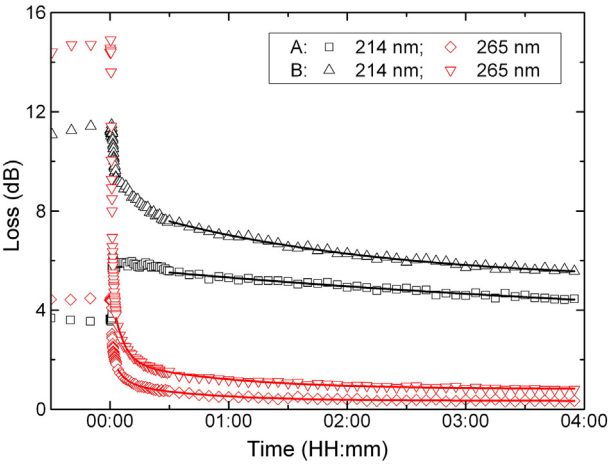

Fig. 7. Kinetics of 214 nm and 265 nm losses during warming-up phase and consecutive recovery at room temperature, after two different processes using the FDP fiber (5 m length): 12 h UV-irradiation and 12 h recovery at 77 K (case A; see Fig. 6, too) and 24 h UV-irradiation (case B); taking the first quick drop not into account, the measured curves for 265 nm (lower curves) can be approximated with two exponential decay functions as follows: $L(t) = 0.65\ dB \cdot \exp(-t/5.0\ min) + 0.71\ dB \cdot \exp(-t/42.0\ min) + 0.34\ dB$ in case A and $L(t) = 2.32\ dB \cdot \exp(-t/5.3\ min) + 1.13\ dB \cdot \exp(-t/55.9\ min) + 0.81\ dB$ in case B with correlation coefficients $r^2 = 0.993$ and 0.995, respectively; after 0.5 h, the measured curves for 214 nm (upper curves) can be approximated with one exponential decay function as follows: $L(t) = 2.18\ dB \cdot \exp(-t/6.0\ h) + 3.0\ dB$ in case A and $L(t) = 2.38\ dB \cdot \exp(-t/1.96\ h) + 5.14\ dB$ in case B, with correlation coefficients $r^2 = 0.967$ and 0.991, respectively.

In first step during the warming-up phase, there were rapid changes of the optical absorption bands at 214 nm and 265 nm within several seconds. There is a sharp drop at 265 nm, especially in case B (>10 dB). On the other hand, the 214 nm loss is sharply reduced in case B (>2 dB) and sharply increased in case A (>2.5 dB). Although the starting values were different, the decay of the absorption band at 265 nm is similar at room temperature. Neglecting the sharp drop and using two decay functions, the time constants during the recovery at room temperature are similar: $t_{d,fast}$ = 5.0 min (A) or 5.3 min (B) and $t_{d,slow}$ = 42 min (A) or 55.9 min (B), with correlation coefficients of $r^2 > 0.95$. On the other hand, the 214 nm loss at room temperature can be approximated with one exponential decay function, after 0.5 h; however, the time constants are different: t_d = 6.0 h (A) or 1.96 h (B). Although no significant changes at the reference wavelength of 330 nm have been observed, the baseline at 214 nm can change during long-term studies slightly influencing the time constants.

Similar behavior in regard to photo-darkening and recovery of 5 m long FDP fiber at different temperatures (77 K and room temperature = 293 K) was observed using the 355 nm HPP laser system. Similar to D_2 lamp damage at different temperatures (Fig. 4), the laser-induced loss of the absorption band at 214 nm is smaller in the order of 8 dB (Fig. 8). On the other hand, the induced 265 nm loss of 1.6 dB was independent at both fiber temperatures used.

After 4 h of UV damage of the 5 m long FDP fiber due to 355 nm laser irradiation, the temporal recovery at different temperatures (77 K and 293 K) is studied (Fig. 9), similar to Fig. 6 with D_2 lamp irradiation. At 77 K, the 214 nm absorption band is decaying from 3.8 dB to 2.6 dB within 12 h; on the other hand, the recovery of the 265 nm optical absorption band is less than 0.2 dB within 12 h.

By warming-up the FUT from 77 K to room temperature, a similar behavior at both wavelengths is observed in accordance to the results shown in Fig. 6. There is a rapid increase of the 214 nm loss of 2.0 dB to a total loss value of 4.6 dB, followed by a recovery to 4 dB, which is approximately linear with time, with a slope value of 0.2 dB/h. On the other hand, the 265 nm band drops rapidly within seconds and decays exponentially with similar time constants $t_{d,\ fast}$ = 2.0 min and $t_{d,\ slow}$ = 30.7 min.

4. Discussion

In all tests, a gain in transmission was observed below 210 nm wavelength when the fibers were cooled to 77 K (see Fig. 5). The absorption edge in silica glass, obeying Urbach's rule, extrapolated, is too small at 200 nm wavelength to explain this effect [15,39]. However, additional extrinsic absorptions due to impurities like chlorine and hydroxyl-groups are limiting the deep-UV transparency. On cooling down the fiber with high OH content core (>600 ppm), in particular,

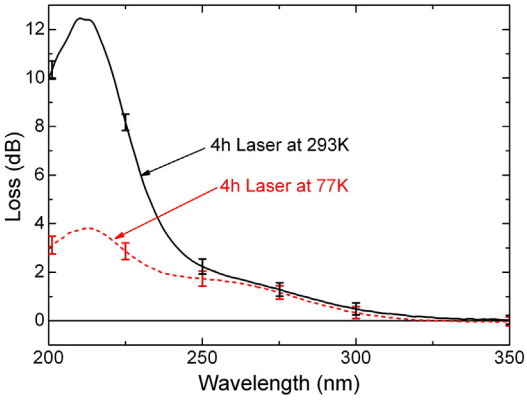

Fig. 8. Comparison of induced loss of the FDP fiber (5 m length) by the 355 nm HPP laser system, at room temperature (293 K, solid line) and 77 K (dashed line).

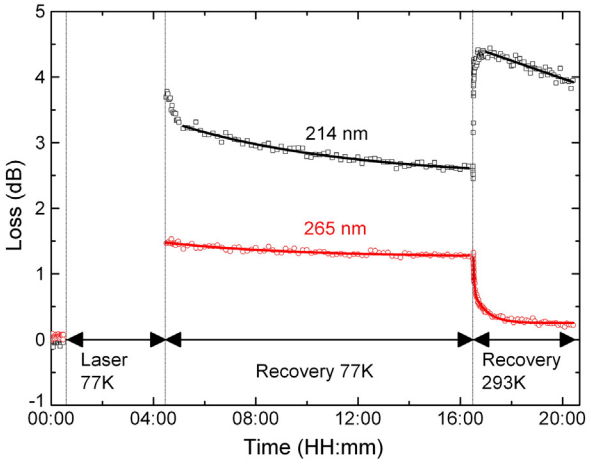

Fig. 9. Kinetics of 214 nm and 265 nm losses of the FDP fiber (5 m length) during 12 h recovery at 77 K and consecutive warming-up phase and recovery at room temperature, after 4 h laser irradiation; the recovery at 77 K can be approximated with one exponential decay function as follows: $L(t) = 0.21\ dB \cdot \exp(-t/5.0\ h) + 1.26\ dB$ for 214 nm and $L(t) = 0.724\ dB \cdot \exp(-t/6.5\ h) + 2.47\ dB$ for 265 nm with correlation coefficients $r^2 = 0.87$ and 0.957, respectively; by taking the first rapid drop not into account, the 265 nm recovery (lower curve) at room temperature was approximated with two exponential decay functions as follows: $L(t) = 0.84\ dB \cdot \exp(-t/2.0\ min) + 0.49\ dB \cdot \exp(-t/30.7\ min) + 0.25\ dB$ with a correlation coefficient $r^2 = 0.992$; after 0.5 h, the measured curves for 214 nm (upper curves) can be approximated linearly as follows: $L(t) = 4.5\ dB - 0.82\ dB/h \cdot t$, with a correlation coefficient $r^2 = 0.854$.

the temperature dependent optical absorption band tail of the strong Si-OH absorption is shifted to a lower wavelength.

Using the broadband D_2 lamp, the E′ center with optical absorption band at 214 nm (5.8 eV) is mainly generated in the improved FDP fiber [10] at room temperature. As indicated in the introduction, the following reactions to generate E′ centers (≡Si•) and non-bridging oxygen hole centers (NBOHC, ≡Si−O•) via a one-photon process with UV light below 220 nm are possible [6,7,14,20], with intrinsic or impurity bonds and precursors P [6,14]:

$$\equiv Si{-}H + h\nu \rightarrow \equiv Si\bullet + H^0 \tag{2}$$

$$\equiv Si{-}Cl + h\nu \rightarrow \equiv Si\bullet + Cl^0 \tag{3}$$

$$\equiv Si{-}O{-}Si\equiv + h\nu \rightarrow \equiv Si\bullet + \bullet O{-}Si\equiv \tag{4}$$

$$P_{E'} + h\nu \rightarrow \equiv Si\bullet. \tag{5}$$

In high OH silica, an additional process for generation of NBOHC is as follows:

$$\equiv Si{-}OH + h\nu \rightarrow \equiv Si{-}O\bullet + H^0. \tag{6}$$

At room temperature (see Figs. 2 and 4), the reaction described in Eqs. (2) and (3) is dominant. Because radiolytic hydrogen due to reactions (2) and (6) and molecular hydrogen from the surrounding atmosphere is present and very mobile, NBOHCs are hardly observed at room temperature. Therefore, the saturation of defects was measured [9,12,37] in standard FVP fibers (1st generation of UV fibers with undoped synthetic silica core and fluorine-doped cladding) and FDP fibers (latest generation of improved UV fibers).

As indicated by the measurement results the main mechanisms of defect generation in high OH silica fibers due to irradiation with a D_2 lamp at 77 K total temperature are different to those at room temperature. First of all, no limits of UV-induced loss at 214 nm and 265 nm were observed up to 12 h irradiation (Fig. 6) and more.

In addition, the UV-induced loss at 214 nm is lower in comparison to the 265 nm loss, even for both UV fibers. Taking the different

lengths into account, the spectral shape and the loss values at the selected wavelengths are nearly the same. Therefore, we can conclude that the reactions (4) and (6) are more dominant at low temperature, leading to a significantly higher concentration of NBOHCs (see Fig. 4). The mobility of radiolytically generated atomic or molecular hydrogen is reduced significantly; therefore, the passivation of the defects generated by the UV light from the D_2 lamp is also reduced. This can be confirmed by the fact, that no saturation of the defects is observed after 12 h or even 24 h of continuous UV irradiation, in contrast to damaging tests at room temperature [9,12,37]. Because there is no dynamic equilibrium between defect generation and passivation at 77 K, we conclude that the passivation of E′ centers and NBOHCs is not thermally activated at cryogenic temperatures.

Using the pulsed 355 nm HPP laser system, with maximum peak power densities of 26 MW/cm^2 below the damage threshold of the optical fiber end faces [1,21], no absorption was observed at the operating wavelength of the laser. On the other hand, the optical absorption bands at 214 nm and 265 nm are generated at room temperature and 77 K. Similar to the D_2 lamp damage at room temperature, these bands can be explained by the E′ center (214 nm, 5.8 eV) and NBOHC (265 nm, 4.8 eV), as described in Ref. [5,7,14]. By using the 355 nm pulsed laser, two damaging mechanism can be taken into account: either by two-photon processes (2·3.5 eV = 7.0 eV, [2,4,33]) or two-step processes on impurity sites [6,7,26]. As shown in Fig. 9, the temporal behavior of optical absorption between 200 nm and 300 nm cannot be monitored during laser irradiation with the implemented setup.

In the following, the recovery at 77 K and after warming-up, the recovery at room temperature will be discussed. In both cases, the broadband D_2 lamp was used for probing (5 s) as described in the experimental setup. At 77 K, only a slight recovery took place, as indicated by the spectral transmission probed with the D_2 lamp. The time constants over 12 h of darkness were determined by least-squares regression (Figs. 6 and 9). The time constants for 214 nm and 265 nm losses are in the order of 5 h (from 4.0 up to 6.3 h). Probing the fiber for 5 s, the loss increase is less than 0.0005 dB at both wavelengths, based on the slope of 0.25 dB/h in Fig. 6.

By taking the fiber out of the Dewar flask, abrupt transmission changes were measured within <30 s. Based on the above data, the loss increase during this warming-up phase under continuous UV irradiation for 135 s is less than 0.02 dB: UV light alone cannot explain the abrupt increases of 214 nm loss (Figs. 6 and 9). Therefore, we conclude that the thermal effects are dominant. The rise time of the temperature is in the same order of <30 s due to the small radius of the fiber (55 μm) and volume to be warmed up. As proposed in Ref. [6,7,14], additional reactions to generate E′ centers are possible:

$$(SiO_2) + n \cdot h\nu \rightarrow (SiO_2)^* \quad (7)$$

$$(SiO_2)^* + P \rightarrow \equiv Si\bullet. \quad (8)$$

In the first step, even at cryogenic temperatures, excited states $(SiO_2)^*$ are generated either due to one-photon absorption (n = 1, D_2 lamp) or due to two-photon absorption (n = 2, 355 nm laser). In the second step, these excited states relax into ground states or transfer their energy to precursors P (see above) to reach the final defect, the E′ centers. In our case, the E′ centers are thermally activated in the presence of excited states, which are generated at 77 K by both UV light sources (Eq. (7)), due to the transformation from precursors P according to Eq. (8).

On the other hand, the abrupt reduction of NBOHC at 265 nm during the warming-up phase and the consecutive recovery at room temperature are based on the following equation, in the presence of molecular hydrogen:

$$\equiv Si\text{–}O\bullet + H_2 \rightarrow Si\text{–}OH + H^0. \quad (9)$$

This molecular hydrogen, with a significantly high mobility at room temperature, is already present due to diffusion from the surrounding atmosphere (short diffusion lengths) or produced by dimerization of atomic hydrogen according to Eqs. (2) and (6). For 265 nm, an exponential decay with two different decay functions and time-constants was approximated; the values are in the order of minutes (fast) and hours (low). In addition to the passivation of NBOHC, E′ centers will also be passivated due to the mobile hydrogen.

In addition to the well-established viewpoint about E′ centers with an absorption band around 214 nm and NBOHCs with an absorption band around 265 nm, the measurement results show similarities to relatively recent developments in the same field [20]. In the wavelength region from 200 nm up to 300 nm, the measured spectral absorption after D_2 lamp irradiation (Figs. 4 and 5) and 355 nm pulsed laser irradiation (not shown in a spectral plot, but also obvious in Fig. 9) is nearly the same in shape (see Figs. 1, 3 and 6 in Ref. [20]). However, the studies have been carried out with high OH synthetic silica bulk samples irradiated by F_2 laser and UV-photobleached at room temperature. Because no electron paramagnetic resonance (EPR) signals have been measured, the authors of Ref. [20] concluded that the NBOHC absorption band is non-Gaussian also covering the deep-UV range, with a significant contribution in the "E′ center" region around 214 nm. As shown in Fig. 6 of Ref. [20], the optical absorption band of dangling bonds in amorphous SiO_2 can be approximated by five Gaussian functions. With our current data on UV fibers with synthetic silica as the core material, the similarities in respect to spectral shape and parallel change of optical attenuation, described in Ref. [20] are really surprising. However, these first fiber-optic results are not sufficient to confirm this new model. Further tests with different steps of temperature difference, starting at liquid nitrogen temperature (77 K) are planned to determine the optical absorption in this wavelength region in more detail.

5. Conclusion

At a cryogenic temperature of 77 K and room temperature, UV defect generation in step-index UV fibers with high OH undoped silica core and F-doped cladding was studied. The photo-darkening between 200 nm and 300 nm was measured using two types of UV sources. Using a broadband D_2 lamp or especially the UV light below 225 nm, the defects are generated by a one-photon process; on the other hand, the 355 nm laser light can generate the same optical absorption due to two-photon absorption or two-step processes. Although different light sources were used, the spectral shape after UV damaging was very similar, at 77 K and room temperature.

Studying the recovery behavior, it was observed that the recovery at 214 nm and 265 nm was small at 77 K. By warming-up the fiber sample to room temperature, the losses changed suddenly, within less than 30 s. While the loss at 265 nm dropped, the loss at 214 nm increased or decreased, depending on the existing defects or precursors before warming up. After the abrupt changes, an additional exponential decay with fast (<5 min) and slow (>1 h) time constants was determined.

By describing the observations, several mechanisms were discussed. Based on the explanations, that the optical absorption band around 214 nm (5.8 eV) is related to E′ centers and around 265 nm (4.7 eV) to NBOHC, mobile atomic and molecular hydrogen was indicated as a major factor; especially in high OH silica, hydrogen can be generated by UV light. Using a new model of oxygen dangling bonds [20] for comparison, the optical absorption measured here showed a surprising congruity. However; because only optical absorption was measurable, the final proof of the new model with our application orientated results is not possible at the moment.

References

[1] G. Hillrichs, C.P. Gonschior, K.-F. Klein, R. Wandschneider, Proc. SPIE 7894 (2011) 0Z.

[2] P. Karlitschek, Fiber-Optic Analyses With UV-Laser-Systems for Noxious Matter Sensor Systems (in German), (PhD thesis) Georg-August Universität, Göttingen, Germany, 1996.
[3] Advanced Optical Technnologies Ltd Basildon UK, Technical Note 9, http://www.aotlasers.com 2004.
[4] R.K. Brimacombe, R.S. Taylor, K.E. Leopold, J. Appl. Phys. 66 (1989) 4035.
[5] D.L. Griscom, J. Non-Cryst. Solids 73 (1985) 51–77.
[6] C. Mühlig, Toward the Absorption of Pulsed ArF Laser Light in Optical Materials of High Transparency (in German), (PhD thesis) Friedrich-Schiller-Universität, Jena, Germany, 2005.
[7] E.J. Friebele, D.L. Griscom, in: M. Tomozawa, R.H. Doremus (Eds.), Treatise on Materials Science and Technology: Glass II, Academic Press St. Louis, 1979, pp. 257–351.
[8] J. Vydra, G. Schötz, Proc. SPIE 3596 (1999) 25.
[9] V.K. Khalilov, K.-F. Klein, J. Belmahdi, R. Timmerman, G.W. Nelson, Proc. SPIE 6083 (2006) 08.
[10] Polymicro Technologies LLC Phoenix AZ USA, Data sheets about UV fibers, http://www.polymicro.com.
[11] J. Assmus, J. Gombert, K.-F. Klein, J.P. Clarkin, G.W. Nelson, Proc. SPIE 3596 (1999) 108.
[12] M. Huebner, H. Meyer, K.-F. Klein, G. Hillrichs, M. Ruetting, M. Veidemanis, B. Spangenberg, J.P. Clarkin, G.W. Nelson, Proc. SPIE 3911 (2000) 303–312.
[13] K.-F. Klein, S. Huettel, R. Kaminski, J. Kirchhof, S. Grimm, G.W. Nelson, Proc. SPIE 3262 (1998) 150.
[14] L. Skuja, J. Non-Cryst. Solids 239 (1998) 16–48.
[15] L. Skuja, H. Hosono, M. Hirano, Proc. SPIE 4347 (2001) 155.
[16] H. Imai, H. Hirashima, J. Non-Cryst. Solids 179 (1994) 202–213.
[17] K.-F. Klein, P. Schließmann, E. Smolka, G. Hillrichs, M. Belz, W.J.O. Boyle, K.T.V. Grattan, Sens. Actuators, B 39 (1997) 305–309.
[18] V.A. Radzig, V.N. Bagratashvili, S.I. Tsypina, P.V. Chernov, A.O. Rybaltovskii, J. Phys. Chem. 99 (1995) 6640–6647.
[19] M. Cannas, S. Costa, R. Boscaino, F.M. Gelardi, J. Non-Cryst. Solids 337 (2004) 9–14.
[20] L. Skuja, K. Kajihara, M. Hirano, H. Hosono, Phys. Rev. B 84 (2011) 205206.
[21] F. Messina, M. Cannas, J. Non-Cryst. Solids 355 (2009) 1038–1041.
[22] J. Kirchhof, P. Kleinert, W. Radloff, E. Below, Phys. Status Solidi A 101 (1987) 391–401.
[23] J. Stone, J. Lightwave Technol. 5 (1987) 712–733.
[24] K.-F. Klein, G. Hillrichs, P. Karlitschek, K.R. Mann, Proc. SPIE 2966 (1996) 564–573.
[25] R.S. Taylor, K.E. Leopold, R.K. Brimacombe, S. Mihailov, Appl. Optics 27 (1988) 3124–3134.
[26] F. Messina, M. Cannas, R. Boscaino, J. Phys. Condens. Matter 20 (2008) 275210.
[27] P. Karlitschek, G. Hillrichs, K.-F. Klein, Opt. Commun. 116 (1995) 219–230.
[28] E. Takala, K.F. Klein, B. Bordini, L. Bottura, J. Bremer, L. Rossi, Cryogenics 52 (2011) 77–81.
[29] E. Takala, The Laser Quenching Technique for Studying the Magneto-Thermal Instability in High Critical Current Density Superconduction Strands for Accelerator Magnets, (PhD thesis) University of Turku, Turku, Finland, 2012.
[30] F. Messina, M. Cannas, J. Non-Cryst. Solids 353 (2007) 522–525.
[31] M. Cannas, F. Messina, J. Non-Cryst. Solids 351 (2005) 1780–1783.
[32] InnoLight GmbH Hannover Germany, Data sheets about diode-pumped semiconductor lasers, http://www.innolight.de.
[33] Coherent Inc., Santa Clara, CA USA, Data sheets about detector systems for lasers, http://www.coherent.com.
[34] LTB Lasertechnik Berlin GmbH Berlin Germany, Data sheets about detector systems for lasers, http://www.ltb-berlin.de.
[35] Heraeus Noblelight GmbH Hanau Germany, Data sheets about deuterium lamps, http://www.heraeus-noblelight.com.
[36] Ocean Optics Inc., Dunedin, FL, USA, Data sheets about fiber-optic spectrometers, http://www.oceanoptics.com.
[37] K.-F. Klein, C.P. Gonschior, H.S. Eckhardt, M.B. Klein, V.K. Khalilov, J. Shannon, Proc. SPIE 8775 (2013) 10.
[38] Hamamatsu K K Hamamatsu Japan, Data sheets about deuterium lamps, http://www.hamamatsu.com.
[39] C.W. Bates Jr., Appl. Opt. 15 (1976) 2976–2978.